Draft version December 10, 2024
Typeset using LaTeX twocolumn style in AASTeX631

The Case for Edge-On Binaries: An Avenue Toward Comparative Exoplanet Demographics

Joseph E. Hand [1,2,*] Konstantin Gerbig [2] and Malena Rice [2]

[1] Department of Physics and Astronomy, University of Kansas, Lawrence, KS 66045, USA
[2] Department of Astronomy, Yale University, New Haven, CT 06511, USA

ABSTRACT

Most Sun-like and higher-mass stars reside in systems that include one or more gravitationally bound stellar companions. These systems offer an important probe of planet formation in the most common stellar systems, while also providing key insights into how gravitational perturbations and irradiation differences from a companion star alter the outcomes of planet formation. Recent dynamical clues have begun to emerge that reveal systematic, non-random structure in the configurations of many planet-hosting binary systems: in close- to moderate-separation ($s < 800$ au) binary star systems, the orbits of exoplanets around individual stellar components are preferentially aligned with the orbital plane of their host stellar binary. In this work, we flip this narrative and search for nearby, edge-on binary star systems that, due to this preferential alignment, are top candidates for radial velocity exoplanet searches. We present a sample of 475 moderate-separation, relatively bright ($G < 12$) *Gaia*-resolved binary star systems in likely near-edge-on configurations. Using a simulated population of exoplanets drawn from transit survey occurrence rate constraints, we provide an overview of the expected planet yields from a targeted search in these systems. We describe the opportunities for comparative exoplanet demographics in the case that *both* stars can be inferred to host edge-on planetary systems – a configuration toward which the presented sample may be biased, given recent observations of orbit-orbit alignment in exoplanet-hosting binary systems.

1. INTRODUCTION

A sizable fraction of all stars are found in systems with one or more bound stellar companions, such that the role of stellar binarity cannot be ignored when interpreting exoplanet demographics. Companion stars may play an important dynamical role both during and after planet formation, sculpting the exoplanet populations in such systems. Beyond providing a dynamical probe, binary star systems also offer the potential to unveil foundational trends in the outcomes of planet formation, given the opportunity of a "control sample" as both stars form in roughly the same conditions and at the same time.

Despite detection biases that disfavor their identification in many large-scale surveys, exoplanet-hosting binary star systems are likely omnipresent across the local solar neighborhood (Hirsch et al. 2021). Blending of sources can obfuscate radial velocity (RV) signals while reducing the observed transit depth in photometric surveys, making exoplanets especially difficult to identify in these systems. Nevertheless, hundreds of confirmed and candidate circumstellar exoplanets (on $s-$type orbits) in binary star systems have been identified to date, largely through observations from the space-based *Kepler* (Borucki et al. 2010) and Transiting Exoplanet Survey Satellite (TESS; Ricker et al. 2015) missions.

Recent studies of these systems have shown that, considering systems from both *Kepler* (Dupuy et al. 2022) and TESS (Christian et al. 2022; Zhang et al. 2023; Christian et al. 2024), the orbits of transiting exoplanets are preferentially aligned with the orbit of their host stellar binary – a configuration that we will call "orbit-orbit alignment", following Rice et al. (2024). Intriguingly, this trend persists from close-in separations (Lester et al. 2023) up to relatively wide sky-projected separations of $s \sim 800$ au, where primordial alignment during star formation should be inefficient (e.g. Bate et al. 2010). The observed alignment potentially reflects dynamical processes, such as dissipative precession during the protoplanetary disk phase (Foucart & Lai 2014; Zanazzi & Lai 2018; Gerbig et al. 2024), or it may instead arise from primordial sources of alignment (Bate 2018). Notably, the orbit-orbit alignment trend appears to strengthen for decreasing primary-to-companion mass ratio (Gerbig et al. 2024), as well as relatively small (non-hot Jupiter) short-period exoplanets (Christian et al. 2024).

[*] Dorrit Hoffleit Undergraduate Research Fellow

In this work, we build upon the observed alignment trend to consider the implications for future surveys. We leverage constraints from the *Gaia* astrometric mission (Gaia Collaboration et al. 2016) to identify all bright edge-on binary star systems in the local solar neighborhood. Given that short-period exoplanet orbits for moderate- to wide-separation binaries tend to be well-aligned with the orbit of their host binary, these systems are ideal candidates for exoplanet RV searches, which have maximized signals for near-edge-on orbital configurations. The sample should also include an enhanced rate of transiting exoplanets, with the exact numbers determined by the orbital separation and eccentricity of planets present within the systems, as well as the degree to which they deviate from exactly edge-on. A unique advantage of our approach is that the resulting sample may enable direct comparison of planetary systems within moderately-wide binary systems: if both stars host near-edge-on planetary systems, the planets around each star can be directly compared to provide insights into how environmental factors influence planet formation.

We note that not all binary exoplanet-hosting systems are expected to exhibit enhanced population-level alignment: in the case that the mutual inclination between orbits is sufficiently large, secular von Zeipel-Lidov-Kozai (ZLK) interactions between the between binary companion and formed planets may further misalign the system (Naoz et al. 2012; Naoz 2016; Zhang et al. 2018). Hints toward this trend have been observed (Rice et al. 2024), but primarily in hot-Jupiter-hosting systems that are intrinsically rare. Our focus is on the most common systems – primarily those with lower-mass exoplanets – which show a stronger trend toward alignment (Christian et al. 2024) and which lack clear signatures indicative of ZLK oscillations that are seen in the hot Jupiter population.

Our work is outlined as follows. In Section 2, we discuss the selection criteria used to construct our sample of edge-on binary systems that exhibit the key properties of promising exoplanet hosts. In Section 3, we describe the projected yield of exoplanets from a search in these systems. We summarize our findings and further discuss the opportunities presented by this sample in Section 4.

2. BUILDING A SAMPLE: EDGE-ON BINARIES AMENABLE TO RV FOLLOW-UP

2.1. *Initial sample selection*

Our sample was drawn from the El-Badry et al. (2021) catalog of 1.8 million binary star systems, identified using photometric and astrometric constraints from the *Gaia* Early Data Release 3 (eDR3; Gaia Collaboration et al. 2021). All binaries in the sample have high-precision astrometric measurements from the *Gaia* mission, and they have been vetted by El-Badry et al. (2021) to demonstrate that the binary components have parallaxes consistent with each other and relative proper motions consistent with a Keplerian orbit. A color-magnitude diagram of the full initial sample is shown in Figure 1.

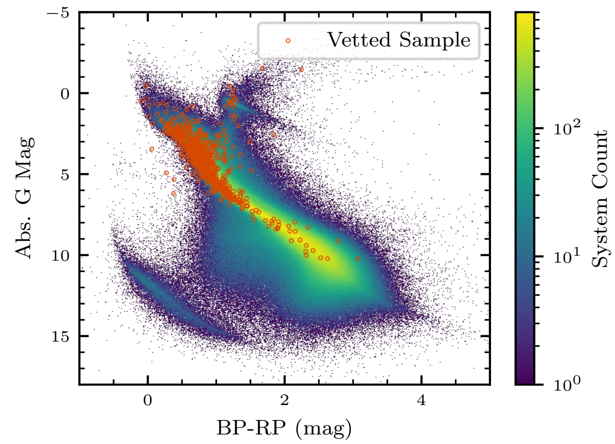

Figure 1. A color-magnitude diagram of stars in the El-Badry et al. (2021) binary catalog, including both the primary and secondary stars in each system. The overlaid red points show stars included in our vetted sample of edge-on binaries.

We downselected from this broader set of binaries based on (1) the sky-projected relative velocities of the stars in each system – specifically, checking whether the binaries are consistent with edge-on orbits; (2) the sky-projected separation between the two stellar components; and (3) the magnitudes of the two stellar components, to restrict our sample to stars that are relatively bright and hence more favorable for RV follow-up observations. We detail each cut in the following paragraphs.

First, we applied a cut to remove binaries that are inconsistent with an edge-on configuration. We used the sky-projected orbit angle, γ (adopted from e.g. Tokovinin & Kiyaeva (2015), Behmard et al. (2022), and Rice et al. (2024)), to carry out this initial vetting step. γ is the angle between the two stars' relative position on the sky $\boldsymbol{r}$ and their relative proper motion vector $\boldsymbol{v}$, i.e.

$$\gamma = \arccos\left(\frac{\boldsymbol{r}\cdot\boldsymbol{v}}{|\boldsymbol{r}||\boldsymbol{v}|}\right). \quad (1)$$

In a perfectly edge-on system, $\gamma = 0°$ or $\gamma = 180°$, depending on the orbital phase at the time of measurement, whereas non-edge-on orientations produce intermediate values of γ. Thus, γ can be used for an initial

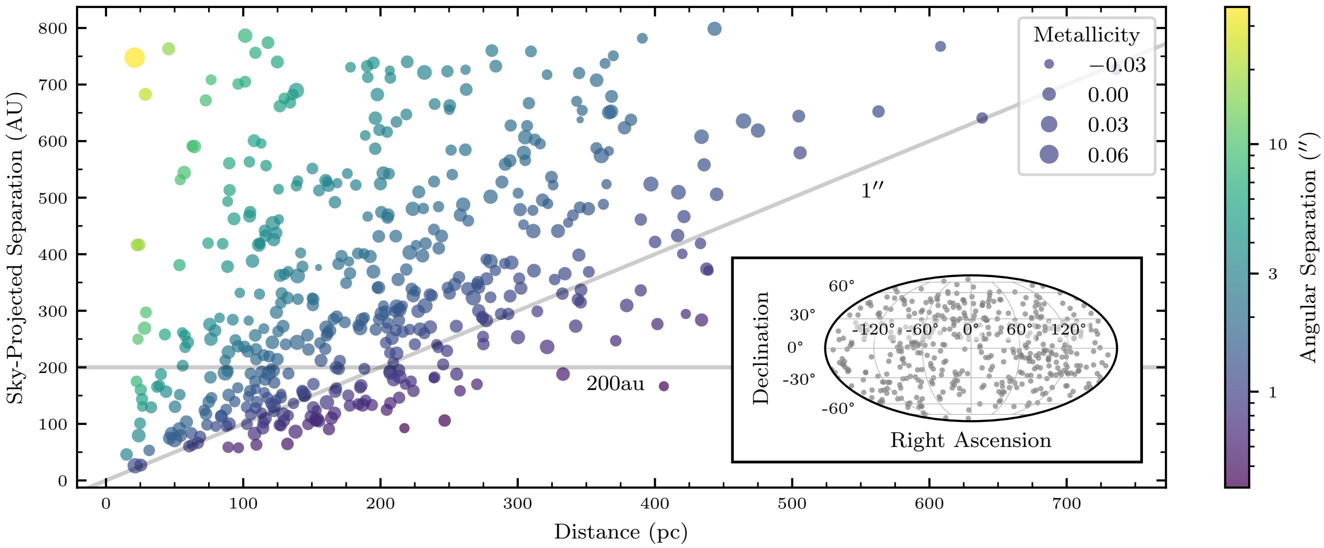

Figure 2. Sky-projected separation of the systems in the final sample, plotted against their distance. Also shown is the angular separation of the stars and their metallicity calculated using `isoclassify`. Two gray reference lines are shown, representing a 200 au sky-projected separation – indicating the rough (non-sky-projected) binary separation below which exoplanet occurrence is suppressed (Moe & Kratter 2021) – and a $1''$ angular separation between the two binary components, which roughly corresponds to the ground-based seeing limit imposed by atmospheric turbulence. The inset figure in the bottom right shows a Mollweide-projected sky map of the stars in our final sample.

selection of systems that are consistent with an edge-on orientation while circumventing a full orbit fit. We calculated γ for each system using the mean values of their astrometric properties as measured by *Gaia* and drawn from El-Badry et al. (2021). Systems where γ was not consistent with either 0° or 180° within 10° were excluded. After removing these, we were left with 189,585 systems.

Second, we restricted our sample to binary systems with a sky-projected separation $s < 800$ AU. This choice was set following Gerbig et al. (2024), to match the empirically-determined separation beyond which a population-level preference for orbit-orbit alignment is no longer confidently observed. Under the assumption that the trend in Christian et al. (2022) and Dupuy et al. (2022) is sufficiently generalizable, exoplanets in these systems are expected to lie on preferentially edge-on orbits, while those in wider binaries would be better represented by isotropy. After this step, the sample was further reduced to 30,246 systems.

Lastly, we excluded systems in which either component has *Gaia* magnitude $G \geq 12$. Both stars in each system should therefore be bright and relatively amenable to RV follow-up. This cut brought our list down to 1,019 systems.

2.2. *Refining the sample with isoclassify and LOFTI*

We further refined our sample by fitting the orbits for each of the 1,019 systems identified from our initial cuts, further constraining the inclination of each system. We leveraged the `lofti_gaia` Python package (Pearce et al. 2020), based on the Orbits For The Impatient (OFTI) algorithm presented in Blunt et al. (2017), to conduct these orbit fits. `lofti_gaia` generates random orbital parameters using the distributions expected under isotropy, then accepts or rejects samples based on a comparison with *Gaia* astrometric constraints for that system, producing a posterior distribution of accepted orbits. To carry out these orbit fits, `lofti_gaia` requires input masses for each modeled star.

We applied the `isoclassify` Python package (Huber 2017; Huber et al. 2017; Berger et al. 2020) to derive stellar masses, radii, and metallicities with associated uncertainties for all stars in our sample. `isoclassify` uses a grid-based approach to derive stellar parameters by mapping isochrones to a set of input observables. Photometry from the *Gaia* G, R_P, and B_P bands, as well as parallax measurements, were included as inputs. We applied the `isoclassify` grid mode via a two-step precess to ensure it converged for all systems. First, the photometric uncertainties were inflated to 0.3 magnitudes and `isoclassify` was applied once. This provided a converged result for all but 23 systems, whose photometric uncertainties were further inflated to 1.0 before re-applying `isoclassify`.

After deriving stellar masses and associated uncertainties, we ran `lofti_gaia` fits with 200 posterior samples accepted per system, drawing all astrometric parameters directly from the El-Badry et al. (2021) binary star catalog. From this, we derived inclinations and uncertainties for each stellar binary system, excluding 7 that failed to converge (likely indicating poor astrometric solutions). Because the inclination posteriors deviate significantly from Gaussian, we define our reported binary inclinations and uncertainties as the 50th percentile of the distribution (i) and the difference between that value and the 68th ($\sigma_{i,\mathrm{upper}}$) and 16th ($\sigma_{i,\mathrm{lower}}$) percentile. Of the remaining 1,012 converged systems, we select the highest-confidence edge-on systems, with $85^\circ < i < 95^\circ$, $\sigma_{i,\mathrm{upper}} < 10^\circ$, and $\sigma_{i,\mathrm{lower}} < 10^\circ$, as our final sample, resulting in 475 systems.

2.3. *Final sample overview*

Our final sample, with properties listed in Table 1, consists of 475 binary star systems. In each system, both stars have $G < 12$, and the components have a sky-projected separation $s < 800$ AU. The 950 stars in our sample (including both primary and secondary stars), overlaid on the full El-Badry et al. (2021) catalog, are shown in Figure 1. The properties of the sample, including the distribution of systems across the sky, are shown in Figure 2. The distribution of inclination uncertainties and stellar effective temperatures represented in the sample are provided in Figure 3.

3. PROJECTED EXOPLANET YIELD

To determine the projected exoplanet yield, we modeled the projected radial velocity and transit signals anticipated under the assumption of a *Kepler*-like distribution of exoplanets (Kunimoto & Matthews 2020) (Section 3.1). We leveraged this simulated population to demonstrate the recoverability of exoplanets within the sample (Sections 3.2 and 3.3), and we discuss the potential of searches for longer-period exoplanets in Section 3.4. Finally, we identified and discuss the known exoplanets in the sample (Section 3.5).

3.1. *Generating a simulated short-period sample*

First, we simulated the projected detection rate for an exoplanet survey across our full sample. Throughout this section, we assume an underlying planet population with properties comparable to those observed in known single-star systems. While exoplanet occurrence rates are lower in close binary systems (Hirsch et al. 2021), binary companions with separation $a > 200$ au have negligible observed impact on the exoplanet occurrence around each star (Moe & Kratter 2021). Our sample includes some binaries with $s < 200$ au; however, these are minimum, sky-projected separations and therefore

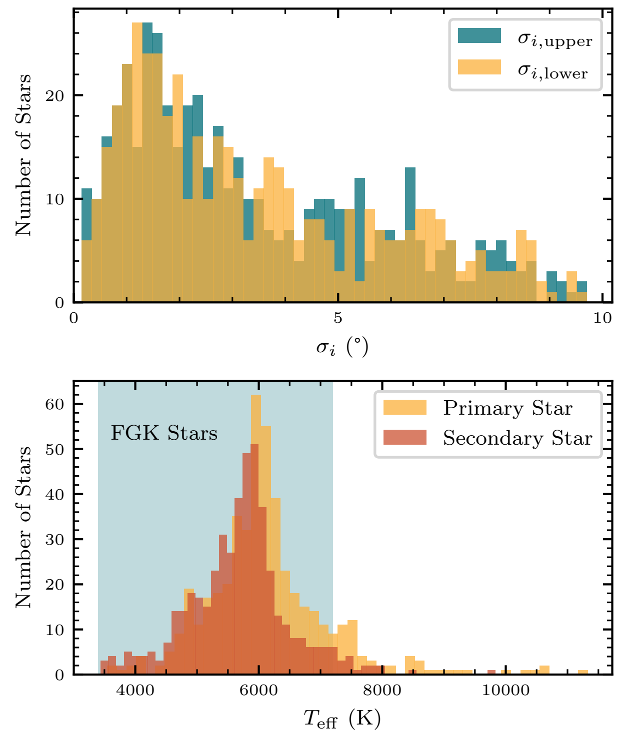

Figure 3. *Top:* Upper and lower asymmetric uncertainties of the system inclinations in our edge-on binaries sample, calculated using `lofti_gaia`. *Bottom:* Effective temperatures of the stars, calculated from *Gaia* photometry using `isoclassify`. The range of temperatures compatible with FGK-type stars is shaded in blue.

may still represent compelling search targets in many cases. Nevertheless, we include a conservative $s = 200$ au line in Figure 2 for reference, and we report values considering both our full sample and the $s > 200$ au sample.

We consider only short- to medium-period ($P < 400$ days), small ($< 6R_\oplus$) exoplanets when determining our projected detection rates. Specifically, our estimates include the parameter space spanned by both the occurrence rate estimates of Kunimoto & Matthews (2020) and the mass-radius relation from Parviainen et al. (2023). The restriction to small planets may underestimate the true exoplanet yield: if higher-mass aligned exoplanets also reside in our sample, they would be more easily identified through an RV search. On the other hand, the observed trend toward alignment may be weakened for giant, hot Jupiter exoplanets (Christian et al. 2024), such that their inclusion within our aligned sample could lead to an overestimated detection rate. Furthermore, short-period giant planets are relatively rare – found around only $\sim 1\%$ of stars (Wright et al. 2012; Fressin et al. 2013; Wittenmyer et al. 2020;

Beleznay & Kunimoto 2022) – such that the majority of detected exoplanets would most likely be smaller. Therefore, we do not expect that the inclusion of these short-period giant planets would significantly change our projected yields. We comment further on wider-orbiting planets in Section 3.4.

For consistency with the Kunimoto & Matthews (2020) occurrence rates, we consider only main-sequence, FGK stars in our yield analyses. As shown in Figure 3, the majority of the stars in our edge-on binaries sample (886/950) lie within the FGK temperature range, with a small tail toward hotter stars. We removed 50 additional potentially post-main-sequence stars through a sample cut to $\log g > 4.0$ dex, though we note that these targets could also be useful to search for exoplanets that are less well-represented by the current census. This leaves 836 stars remaining. Kunimoto & Matthews (2020) provides three different distributions of exoplanet occurrence rates for F, G, and K type stars. We accordingly divided our sample into these three categories based on their $T_{\rm eff}$, as determined by `isoclassify`.

We generated a set of 14, 37, and 57 exoplanets for each F, G, and K star in our sample, respectively. These numbers were chosen to be 30× the average number of exoplanets per star of each classification, as measured in Kunimoto & Matthews (2020). Each exoplanet was assigned a radius and period by randomly selecting a radius-period bin from Kunimoto & Matthews (2020) for the host stellar type, weighted by the bins' mean probability. A point was then drawn at random from this bin according to a logarithmic uniform distribution. For bins with only upper-limit occurrence rates provided, we set the mean to 0 (corresponding to a 0% chance of drawing a planet from that bin).

We then used the `spright` Python package (Parviainen et al. 2023) to assign masses to the planets, leveraging empirical constraints on the mass-radius relationship for small exoplanets ($R < 6R_\oplus$). For each planet, three orbital inclinations were adopted using three distinct orbit-orbit alignment schemes: perfect alignment with the host binary's orbit, 20° dispersion around perfect alignment (drawing from a Gaussian distribution with $1\sigma = 20°$, in accordance with the observed trend from Christian et al. (2022) for systems with $s < 800$ au), and random/isotropic alignment, drawn from a $\sin i$ distribution for comparison with field stars. This process resulted in a sample of 23,859 randomly generated exoplanets matching observed demographics.

3.2. *Expected short-period planet RV signals*

The RV signals from our simulated sample are shown in the left panel of Figure 4. As anticipated, the aligned population produces systematically higher-amplitude RV signals than an isotropic distribution.

We predict yields for an RV survey by identifying how many exoplanets in our generated sample meet a set of detection criteria, then dividing by 30 to correct for the inflated number of exoplanets generated (see Section 3.1) and converting to percent yields. Considering the full sample (836 stars), we predict yields of 52%, 3.2%, and 0.6% for companion planets with RV semi-amplitude $K > 1$, 5, and 10 m/s, respectively. Excluding systems with $s < 200$ au (leaving 577 stars), these estimates were reduced to 47%, 2.8%, and 0.3%.

Though many of our simulated signals lie well above the instrumental noise limits of current-generation extreme-precision radial velocity spectrographs ($\sim 10-30$ cm/s), a substantive fraction cannot be recovered in practice. One limiting factor is the achievable RV precision: spectrographs typically achieve lower RV precision for stars above the Kraft break ($T_{\rm eff} > 6250$ K; Kraft 1967) due to Doppler broadening, precluding the detection of most small exoplanets modeled in this work. Considering this limitation, we provide more conservative estimates of exoplanet yields by excluding all stars above the Kraft break from our full sample (leaving 675 stars), resulting in yields of 60%, 3.5%, and 0.6% for $K > 1$, 5, and 10 m/s, respectively. Excluding systems with $s < 200$ au (leaving 448 stars) reduces these estimates to 55%, 3.1%, and 0.4%.

Another limiting factor is stellar activity, which provides an astrophysical noise source that may mask low-amplitude RV signals. The impact of stellar jitter can be assessed by obtaining vetting spectra prior to initiating a full survey – for example, via near-infrared spectroscopy using the $\log R'_{\rm HK}$ index (Noyes et al. 1984). Adopting a requirement that $\log R'_{\rm HK} < -4.75$ – indicating relatively inactive stars – and considering the population-level distribution of $\log R'_{\rm HK}$ values for FGK stars identified in Gomes da Silva et al. (2021), we anticipate that ∼67% of our identified sample would remain.

3.3. *Short-period transit likelihood*

The bias of our sample toward a near-edge-on-configuration also implies that, if the exoplanets are well-aligned with their host stellar binary orbit, they should have a relatively high likelihood of transiting. Therefore, we quantify the transit rate anticipated within our simulated sample, together with the expected transit depths for our exoplanets, with results shown in the right panel of Figure 4. The median expected transit

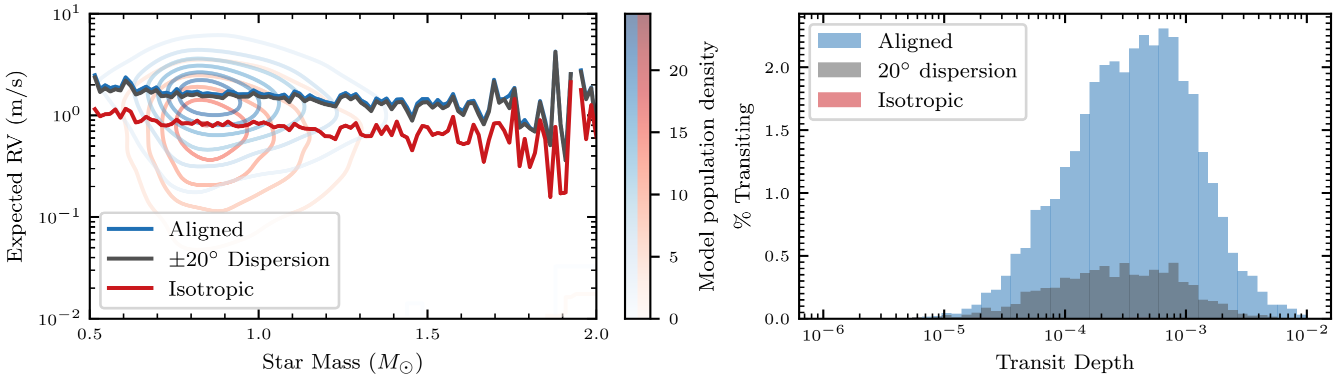

Figure 4. Simulated exoplanet signals expected for our full edge-on binaries sample. When systems with $s < 200$ au are excluded from the sample, the distributions are not substantially affected. *Left:* Semi-amplitudes of the modeled RV signals as a function of host star mass, assuming three different population-level alignment distributions: perfect alignment (*blue*), 20°, dispersion (*grey*), and random/isotropic alignment (*red*). The contours show the distribution of all models, while the dark lines show the mean RV amplitude within each host mass bin. As expected, the RV amplitude decreases with increasing host star mass. There is a significant difference between the isotropic alignment scheme, which would be expected for field stars, and the other two alignment schemes, expected for the edge-on binaries in our sample. *Right:* The expected transit signals from the simulated exoplanet population, assuming the same alignment schemes. The aligned exoplanets are significantly more likely to transit than the isotropically oriented ones.

duration for the sample is 3.3 hours, and 90% of transits have durations between 1.1 and 9.5 hours.

We find that 7.1% of simulated planets transit when assuming a 20° dispersion from alignment with their host star, compared with 0.1% transiting for isotropic orientations and 36.8% without dispersion. However, the expected transit depths are relatively shallow – with a peak likelihood around 500 ppm – such that they likely would not have been captured by previous transit surveys. For reference, only 478 of the 6156 TOIs on the TESS Project Candidates list (accessed November 15, 2024), excluding false positives, fall at or below this threshold.

Targets within our list are spread across the sky (see inset of Figure 2) – that is, mostly outside of the *Kepler* field (Borucki et al. 2010) – and, while most have been observed by the TESS mission, the angular separation between stars is smaller than the TESS pixel size (21″) in nearly all cases, such that our sample would suffer from severe blending. Therefore, despite the high anticipated transit rate, past surveys likely would not have found most transiting planets within our sample.

We predict the fraction of stars in our sample exhibiting transit signals observable with 1 m ground-based telescopes, with a transit depth threshold of 700 ppm (Mallonn et al. 2022). In the full sample, including stars in systems with $s < 200$ au, 1.5% of systems have transit signals observable by ground-based instrumentation, assuming 20° dispersion. Excluding systems with $s < 200$ au, this estimate is reduced to 1.4%.

3.4. *Longer-period planets*

Our simulations include only the signals of short-period, low-mass planets. This is motivated by three primary considerations: (1) the trend toward alignment was found specifically for transiting planets, so that it is unclear whether the trend extends to wider-orbiting planets; (2) based on projected occurrence rates that indicate a paucity of short-period giant planets, small exoplanets would likely constitute the bulk of discoveries at short orbital periods; and (3) short-period planets can be discovered most efficiently, on a timeline of $\lesssim 3$ years, through RV surveys.

If our stellar binaries form via disk fragmentation (see e.g. Offner et al. (2023)), or if dissipative precession operates to align these systems (see Gerbig et al. (2024)), however, we may expect that wider-orbiting planets should follow the same orbit-orbit trends observed for the transiting population. As such, a longer-term RV survey for wide companions may also have excellent potential for the discovery of additional planets: long-period giant planets have relatively large RV signals and are found around $\sim 30\%$ of FGK stars (e.g. Fernandes et al. 2019). We also note that our identified population, given its relative proximity, would be an excellent target group to search for astrometric planet candidates with datasets such as upcoming *Gaia* releases (Espinoza-Retamal et al. 2023; Feng 2024).

3.5. *Cross-referencing with known exoplanets/TOIs*

To search for known planets in our sample, our full 950-star sample was cross-referenced against the NASA Exoplanet Archive "Planetary Systems" (NASA Exoplanet Archive 2024) table and the TESS Objects of Interest (TOI; Guerrero et al. 2021) catalogue, both accessed on November 15, 2024. With a $20''$ search radius around each star, we identified one confirmed exoplanet in the final sample: HD 39855 b, a short-period, non-transiting exoplanet confirmed by Feng et al. (2019). The absence of additional known transiting exoplanets is unsurprising given the sample size and properties (see Section 3.3). In addition to HD 39855 b, two TOIs were identified within the sample: TOI-2422.01 and TOI-4175.01, with TFOP WG dispositions (Akeson & Christiansen 2019) of "ambiguous planetary candidate" and "planetary candidate," respectively.

HD 39855 b has a minimum mass consistent with that of a super-Earth or sub-Neptune ($M_p \sin i = 8.5 \pm 1.5 M_\oplus$; Feng et al. 2019), and our analyses show that the stellar binary has a sky-projected separation $s \sim 250$ au with inclination $i = 93^{+5^\circ}_{-1}$. In the case that HD 39855 b lies on an edge-on orbit that is roughly collinear with its binary host system, the minimum mass would be close to the true mass of the planet. Calculating $\sin i$ for the 200 posterior inclination samples from `lofti_gaia` and deriving new posteriors from this distribution, we estimate that $\sin i = 0.96^{+0.04}_{-0.15}$ for HD 39855 b under the assumption of orbit-orbit alignment with a 20° dispersion, corresponding to a true exoplanet mass $9.3^{+2.6}_{-1.9} M_\oplus$.

4. DISCUSSION

In this work, we identified a sample of *Gaia*-resolved, edge-on binary star systems that, based on the observed orbital geometries of exoplanets in similar systems, are predicted to host an overabundance of edge-on planetary systems (Table 1). Our identified systems therefore constitute a promising sample to search for exoplanets through RV or transit observations, which are most sensitive to near-edge-on configurations. We showed that, if these systems are well-aligned with their binary hosts' orbits, a survey of these targets should have a significantly higher yield of exoplanet detections, through both RV and transit searches, than would be expected for a blind search across field stars – quantified explicitly in Section 3.

If the observed orbit-orbit alignment trend persists, these systems would offer a unique capability to conduct *comparative* demographic studies within binary exoplanet systems. Orbit-orbit aligned systems, with $i \sim 90^\circ$ for planetary systems around both stars, have the potential to enable direct comparisons of exoplanet populations across pairs of stars that formed under similar initial conditions. Such a comparison would offer fundamental insights into the stochasticity of planet formation, informing whether stars formed in similar environments tend to form similar planets.

Another useful future direction would be the derivation of stellar inclinations for the edge-on binaries sample. Several precisely spin-orbit and orbit-orbit aligned exoplanet-hosting binary systems were previously found in Rice et al. (2023) and Rice et al. (2024), suggesting the absence of previous dynamical excitation in those systems. Full alignment would be expected if the stellar binary formed via disk fragmentation (see e.g. Offner et al. 2023) or if dissipative precession aligned the system while spin-orbit misalignment was never excited, as explored in Gerbig et al. (2024). While the orbital inclinations of non-transiting exoplanet systems cannot be directly inferred, a combination of an edge-on orbital configuration and an edge-on stellar rotation configuration – indicating two axes of alignment – would lend confidence to the hypothesis that any identified planets formed quiescently, with an orbit that is also edge-on and that has not undergone significant dynamical excitation to misalign the system (e.g. Su & Lai 2024).

Stellar inclinations can be derived through a combination of photometric stellar rotation periods and spectroscopic $v \sin i_*$ measurements. While rotation periods can only be inferred for stars with long-lived starspots (e.g. Nielsen et al. 2013) or asteroseismic signals (e.g. Gizon & Solanki 2003; Kamiaka et al. 2018), a subset of our sample may be suitable for either or both methods. Thus, targeted follow-up observations may help to further constrain the 3D orientations of these systems.

5. ACKNOWLEDGEMENTS

We are grateful to the Dorrit Hoffleit Undergraduate Research Scholarship program at Yale University, which provided support for this project. M.R. acknowledges support from Heising-Simons Foundation Grant #2023-4478.

This work has made use of data from the European Space Agency (ESA) mission *Gaia* (https://www.cosmos.esa.int/gaia), processed by the *Gaia* Data Processing and Analysis Consortium (DPAC, https://www.cosmos.esa.int/web/gaia/dpac/consortium). Funding for the DPAC has been provided by national institutions, in particular the institutions participating in the *Gaia* Multilateral Agreement.

This research has made use of the NASA Exoplanet Archive, which is operated by the California Institute of Technology, under contract with the National Aeronautics and Space Administration under the Exoplanet Exploration Program.

Facilities: Exoplanet Archive, *Gaia*

Software: `astropy` (Astropy Collaboration et al. 2013, 2018, 2022), `isoclassify` (Huber 2017; Huber et al. 2017; Berger et al. 2020), `lofti_gaia` (Pearce et al. 2020), `gnu parallel` (Tange 2023), `matplotlib` (Hunter 2007), `mwdust` (Bovy et al. 2016), `numpy` (Oliphant 2006; Walt et al. 2011; Harris et al. 2020), `pandas` (McKinney 2010), `scipy` (Virtanen et al. 2020), `spright` (Parviainen et al. 2023), `tqdm` (Costa-Luis et al. 2024)

REFERENCES

Akeson, R., & Christiansen, J. 2019, 233, 140.09. https://ui.adsabs.harvard.edu/abs/2019AAS...23314009A

Astropy Collaboration, Robitaille, T. P., Tollerud, E. J., et al. 2013, A&A, 558, A33, doi: 10.1051/0004-6361/201322068

Astropy Collaboration, Price-Whelan, A. M., Sipőcz, B. M., et al. 2018, AJ, 156, 123, doi: 10.3847/1538-3881/aabc4f

Astropy Collaboration, Price-Whelan, A. M., Lim, P. L., et al. 2022, ApJ, 935, 167, doi: 10.3847/1538-4357/ac7c74

Bate, M. R. 2018, MNRAS, 475, 5618, doi: 10.1093/mnras/sty169

Bate, M. R., Lodato, G., & Pringle, J. E. 2010, MNRAS, 401, 1505, doi: 10.1111/j.1365-2966.2009.15773.x

Behmard, A., Dai, F., & Howard, A. W. 2022, AJ, 163, 160

Beleznay, M., & Kunimoto, M. 2022, MNRAS, 516, 75, doi: 10.1093/mnras/stac2179

Berger, T. A., Huber, D., Van Saders, J. L., et al. 2020, AJ, 159, 280

Blunt, S., Nielsen, E. L., De Rosa, R. J., et al. 2017, The Astronomical Journal, 153, 229, doi: 10.3847/1538-3881/aa6930

Borucki, W. J., Koch, D., Basri, G., et al. 2010, Science, 327, 977, doi: 10.1126/science.1185402

Bovy, J., Rix, H.-W., Green, G. M., Schlafly, E. F., & Finkbeiner, D. P. 2016, ApJ, 818, 130

Christian, S., Vanderburg, A., Becker, J., et al. 2022, The Astronomical Journal, 163, 207, doi: 10.3847/1538-3881/ac517f

Christian, S., Vanderburg, A., Becker, J., et al. 2024, arXiv e-prints, arXiv:2405.10379, doi: 10.48550/arXiv.2405.10379

Costa-Luis, C. d., Larroque, S. K., Altendorf, K., et al. 2024, tqdm: A fast, Extensible Progress Bar for Python and CLI, Zenodo, doi: 10.5281/zenodo.13207611

Dupuy, T. J., Kraus, A. L., Kratter, K. M., et al. 2022, Monthly Notices of the Royal Astronomical Society, 512, 648, doi: 10.1093/mnras/stac306

El-Badry, K., Rix, H.-W., & Heintz, T. M. 2021, Monthly Notices of the Royal Astronomical Society, 506, 2269, doi: 10.1093/mnras/stab323

Espinoza-Retamal, J. I., Zhu, W., & Petrovich, C. 2023, AJ, 166, 231, doi: 10.3847/1538-3881/ad00b9

Feng, F. 2024, arXiv e-prints, arXiv:2403.08226, doi: 10.48550/arXiv.2403.08226

Feng, F., Crane, J. D., Xuesong Wang, S., et al. 2019, The Astrophysical Journal Supplement Series, 242, 25, doi: 10.3847/1538-4365/ab1b16

Fernandes, R. B., Mulders, G. D., Pascucci, I., Mordasini, C., & Emsenhuber, A. 2019, ApJ, 874, 81, doi: 10.3847/1538-4357/ab0300

Foucart, F., & Lai, D. 2014, MNRAS, 445, 1731, doi: 10.1093/mnras/stu1869

Fressin, F., Torres, G., Charbonneau, D., et al. 2013, ApJ, 766, 81, doi: 10.1088/0004-637X/766/2/81

Gaia Collaboration, Prusti, T., de Bruijne, J. H. J., et al. 2016, A&A, 595, A1, doi: 10.1051/0004-6361/201629272

Gaia Collaboration, Brown, A. G. A., Vallenari, A., et al. 2021, A&A, 649, A1, doi: 10.1051/0004-6361/202039657

Gerbig, K., Rice, M., Zanazzi, J. J., Christian, S., & Vanderburg, A. 2024, ApJ, 972, 161, doi: 10.3847/1538-4357/ad5f2b

Gizon, L., & Solanki, S. K. 2003, ApJ, 589, 1009, doi: 10.1086/374715

Gomes da Silva, J., Santos, N. C., Adibekyan, V., et al. 2021, A&A, 646, A77, doi: 10.1051/0004-6361/202039765

Guerrero, N. M., Seager, S., Huang, C. X., et al. 2021, ApJS, 254, 39, doi: 10.3847/1538-4365/abefe1

Harris, C. R., Millman, K. J., van der Walt, S. J., et al. 2020, Nature, 585, 357

Hirsch, L. A., Rosenthal, L., Fulton, B. J., et al. 2021, AJ, 161, 134, doi: 10.3847/1538-3881/abd639

Huber, D. 2017, Zenodo, doi, 10

Huber, D., Zinn, J., Bojsen-Hansen, M., et al. 2017, ApJ, 844, 102

Hunter, J. D. 2007, Computing in science & engineering, 9, 90

Kamiaka, S., Benomar, O., & Suto, Y. 2018, MNRAS, 479, 391, doi: 10.1093/mnras/sty1358

Kraft, R. P. 1967, ApJ, 150, 551, doi: 10.1086/149359

Kunimoto, M., & Matthews, J. M. 2020, The Astronomical Journal, 159, 248, doi: 10.3847/1538-3881/ab88b0

Lester, K. V., Howell, S. B., Matson, R. A., et al. 2023, The Astronomical Journal, 166, 166, doi: 10.3847/1538-3881/acf563

Mallonn, M., Poppenhaeger, K., Granzer, T., Weber, M., & Strassmeier, K. G. 2022, Astronomy & Astrophysics, 657, A102, doi: 10.1051/0004-6361/202140599

McKinney, W. 2010, in Proceedings of the 9th Python in Science Conference, Vol. 445, Austin, TX, 51–56

Moe, M., & Kratter, K. M. 2021, MNRAS, 507, 3593, doi: 10.1093/mnras/stab2328

Naoz, S. 2016, ARA&A, 54, 441, doi: 10.1146/annurev-astro-081915-023315

Naoz, S., Farr, W. M., & Rasio, F. A. 2012, ApJL, 754, L36, doi: 10.1088/2041-8205/754/2/L36

NASA Exoplanet Archive. 2024, Planetary Systems, Version: 2024-11-15, NExScI-Caltech/IPAC, doi: 10.26133/NEA12

Nielsen, M. B., Gizon, L., Schunker, H., & Karoff, C. 2013, A&A, 557, L10, doi: 10.1051/0004-6361/201321912

Noyes, R. W., Hartmann, L. W., Baliunas, S. L., Duncan, D. K., & Vaughan, A. H. 1984, The Astrophysical Journal, 279, 763, doi: 10.1086/161945

Offner, S. S. R., Moe, M., Kratter, K. M., et al. 2023, in Astronomical Society of the Pacific Conference Series, Vol. 534, Protostars and Planets VII, ed. S. Inutsuka, Y. Aikawa, T. Muto, K. Tomida, & M. Tamura, 275, doi: 10.48550/arXiv.2203.10066

Oliphant, T. E. 2006, A guide to NumPy, Vol. 1 (Trelgol Publishing USA)

Parviainen, H., Luque, R., & Palle, E. 2023, Spright: a probabilistic mass-density-radius relation for small planets, arXiv, doi: 10.48550/arXiv.2311.07255

Pearce, L. A., Kraus, A. L., Dupuy, T. J., et al. 2020, AJ, 894, 115

Rice, M., Gerbig, K., & Vanderburg, A. 2024, AJ, 167, 126, doi: 10.3847/1538-3881/ad1bed

Rice, M., Wang, S., Gerbig, K., et al. 2023, AJ, 165, 65, doi: 10.3847/1538-3881/aca88e

Ricker, G. R., Winn, J. N., Vanderspek, R., et al. 2015, Journal of Astronomical Telescopes, Instruments, and Systems, 1, 014003, doi: 10.1117/1.JATIS.1.1.014003

Su, Y., & Lai, D. 2024, arXiv e-prints, arXiv:2411.08094, doi: 10.48550/arXiv.2411.08094

Tange, O. 2023, GNU Parallel 20240522 ('Tbilisi'), Zenodo, doi: 10.5281/zenodo.11247979

Tokovinin, A., & Kiyaeva, O. 2015, MNRAS, 456, 2070

Virtanen, P., Gommers, R., Oliphant, T. E., et al. 2020, Nature Methods, 17, 261

Walt, S. v. d., Colbert, S. C., & Varoquaux, G. 2011, Computing in Science & Engineering, 13, 22

Wittenmyer, R. A., Wang, S., Horner, J., et al. 2020, MNRAS, 492, 377, doi: 10.1093/mnras/stz3436

Wright, J. T., Marcy, G. W., Howard, A. W., et al. 2012, ApJ, 753, 160, doi: 10.1088/0004-637X/753/2/160

Zanazzi, J. J., & Lai, D. 2018, MNRAS, 477, 5207, doi: 10.1093/mnras/sty951

Zhang, J., Weiss, L. M., Huber, D., et al. 2023, arXiv e-prints, arXiv:2310.03299, doi: 10.48550/arXiv.2310.03299

Zhang, Y., Li, Q., Xie, J.-W., et al. 2018, ApJ, 861, 116, doi: 10.3847/1538-4357/aac6c3

Table 1. Systems in our edge-on binaries sample, ordered in reverse by angular separation between the two stars. Listed parameters include the *Gaia* DR3 source IDs of the stellar components, along with the coordinates of the primary star ($\mathrm{RA_p}$,$\mathrm{Dec_p}$), the angular and sky-projected separation between the binary components (θ and s, respectively), the *Gaia* G magnitudes (G_p, G_s) and effective temperatures ($T_\mathrm{eff,p}$, $T_\mathrm{eff,s}$) of both stars, and the derived binary inclination (i). Additional columns can be found in the full table.

Prim. Gaia DR3 ID	Sec. Gaia DR3 ID	$\mathrm{RA_p}$ (°)	$\mathrm{Dec_p}$ (°)	G_p	G_s	s (au)	θ ($''$)	$T_\mathrm{eff,p}$ (K)	$T_\mathrm{eff,s}$ (K)	i (°)
6603693881832177664	6603693808817829888	341.24247	−33.25103	10.7	11.8	747	35.82	3674 ± 89	3434 ± 98	$87.1^{+0.9}_{-3.7}$
3053492881541641728	3053492881541639680	113.02360	−8.88207	5.8	9.9	683	23.81	6111 ± 473	4187 ± 129	$90.1^{+0.3}_{-0.2}$
4503423641091792896	4503423641091795968	268.93686	18.50017	8.7	10.8	416	18.50	4444 ± 163	3741 ± 87	$88.3^{+1.0}_{-3.3}$
6840822904599512064	6840822904602986496	328.28073	−12.82863	10.3	11.9	417	17.30	3925 ± 101	3576 ± 85	$94.2^{+6.4}_{-1.5}$
3042300093686461440	3042299715729340928	118.35642	−8.65503	11.3	11.6	763	16.72	4027 ± 106	3943 ± 104	$88.9^{+0.6}_{-2.7}$
2966316109264052224	2966316109264051200	88.62609	−19.70445	7.3	10.1	250	10.73	5269 ± 217	3980 ± 105	$93.1^{+4.9}_{-1.0}$
4290328769993455616	4290328529475286528	296.48926	4.24840	6.9	10.8	297	10.20	5740 ± 275	3883 ± 100	$93.1^{+6.3}_{-1.1}$
2070269864129830400	2070269864129829888	309.65164	44.64113	9.5	10.2	532	9.83	5151 ± 217	4742 ± 190	$87.6^{+0.7}_{-6.4}$
3482326708703712768	3482326708703712768	173.06825	−29.26038	5.5	5.6	269	9.58	6231 ± 548	6183 ± 496	$91.1^{+2.3}_{-0.5}$
3136977596845662208	3136977596847142400	115.87970	3.48546	6.9	10.1	544	9.55	6320 ± 620	4773 ± 181	$90.5^{+0.5}_{-0.5}$
4305953826646567936	4305953826646567424	286.44880	6.54648	6.8	8.7	591	9.41	6858 ± 748	5767 ± 286	$89.1^{+0.5}_{-2.8}$
3623497335919494144	3623497331624720384	199.36348	−10.54622	6.8	11.8	708	9.25	7046 ± 779	4260 ± 145	$91.5^{+2.3}_{-0.7}$
5913288643608847360	5913288643608845312	259.64377	−62.60066	9.3	11.3	672	9.25	5555 ± 238	4460 ± 166	$86.7^{+0.9}_{-6.2}$
6610154852675341312	6610154852675341312	344.45165	−26.10948	7.5	9.0	590	9.18	6087 ± 576	5519 ± 232	$89.8^{+0.3}_{-0.6}$
725398123501434496	725398127796012288	154.30858	23.10578	5.7	10.9	175	7.86	5978 ± 361	3741 ± 86	$91.6^{+4.0}_{-0.8}$
4153991458443776000	4153991458440172032	274.01913	−11.18015	7.6	11.3	786	7.76	6820 ± 910	4970 ± 218	$94.5^{+6.3}_{-1.2}$
4360581000283303424	4360581000283303936	259.99344	−6.42912	9.7	9.9	701	7.28	5637 ± 309	5556 ± 297	$86.0^{+1.6}_{-7.4}$
5567252543129606144	5567252749288699904	95.19632	−44.78881	8.3	10.4	381	7.11	5661 ± 252	4588 ± 174	$90.8^{+2.2}_{-0.4}$
3683354538481468928	3683354542776364032	189.78491	−1.55192	10.4	11.3	705	6.95	5343 ± 221	4843 ± 184	$91.5^{+3.3}_{-2.0}$
5291426101251320832	5291426101251320832	123.44845	−58.61850	8.4	11.7	756	6.95	6535 ± 552	4742 ± 189	$90.1^{+0.9}_{-0.6}$
2695225573198454784	2695225367040024576	325.06825	3.73716	8.4	10.7	774	6.56	6495 ± 556	5369 ± 223	$91.5^{+2.8}_{-1.0}$
3524996177995941888	3525007929026463744	194.43153	−14.46342	8.8	11.7	160	6.32	4565 ± 171	3612 ± 83	$93.1^{+5.4}_{-1.7}$
2909512452354630144	2909512448058315776	91.35280	−28.67771	8.1	8.3	561	6.25	6272 ± 462	6148 ± 405	$87.0^{+1.8}_{-5.7}$
77161217776670208	77161222072044288	32.71752	13.68296	8.0	8.5	258	6.02	5589 ± 239	5368 ± 222	$88.9^{+0.5}_{-1.5}$
1424045373912608256	1424045373911120896	247.18126	51.40777	6.0	11.9	740	5.93	4793 ± 200	4757 ± 180	$90.7^{+3.3}_{-2.0}$
1215046973888838144	1215046973888837632	230.13371	22.10244	9.9	11.5	513	5.70	5466 ± 229	4577 ± 171	$88.7^{+0.7}_{-2.5}$
1880487388297606144	1880487388298464512	337.50836	25.94102	8.3	10.5	420	5.64	5990 ± 354	4866 ± 185	$94.2^{+7.1}_{-1.6}$
951395355544081792	951395355544517120	102.79925	40.49541	9.0	10.3	601	5.57	5949 ± 408	5421 ± 225	$91.1^{+2.6}_{-1.0}$
6065381024758288384	6065381029065308160	205.43621	−54.55954	5.2	6.6	493	5.56	10559 ± 1646	8537 ± 1021	$92.9^{+4.2}_{-1.3}$
984509244157298304	984509244157298432	117.16387	53.64621	8.5	11.5	144	5.47	4736 ± 179	3671 ± 84	$92.5^{+6.3}_{-1.1}$

Note—See an online version of this manuscript for a downloadable version of the full table.